

# Cross-over from retro to specular Andreev reflections in bilayer graphene

Dmitri K. Efetov<sup>1</sup> and Konstantin B. Efetov<sup>2,3</sup>

<sup>1</sup>*Department of Electrical Engineering and Computer Science,  
Massachusetts Institute of Technology, Cambridge, USA*

<sup>2</sup>*Theoretische Physik III, Ruhr-Universität Bochum, D-44780 Bochum, Germany*

<sup>3</sup>*National University of Science and Technology "MISiS", Moscow, 119049, Russia*

(Dated: May 16, 2016)

Ongoing experimental progress in the preparation of ultra-clean graphene/superconductor (SC) interfaces enabled the recent observation of specular interband Andreev reflections (AR)<sup>1</sup> at bilayer graphene (BLG)/NbSe<sub>2</sub> van der Waals interfaces [Nature Physics 12, (2016)<sup>2</sup>]. Motivated by this experiment we theoretically study the differential conductance across a BLG/SC interface at the continuous transition from high to ultra-low Fermi energies  $E_F$  in BLG. Using the Bogoliubov-deGennes equations<sup>3</sup> and the Blonder-Tinkham-Klapwijk formalism<sup>4</sup> we derive analytical expressions for the differential conductance across the BLG/SC interface. We find a characteristic signature of the cross-over from intra-band retro- (high  $E_F$ ) to inter-band specular (low  $E_F$ ) ARs, that manifests itself in a strongly suppressed interfacial conductance when the excitation energy  $|\varepsilon| = |E_F| < \Delta$  (the SC gap). The sharpness of these conductance dips is strongly dependent on the size of the potential step at the BLG/SC interface  $U_0$ .

PACS numbers: 74.45.+c, 73.63.-b

## I. INTRODUCTION

Andreev reflections<sup>1</sup> (AR) at normal metal (N) to superconductor (SC) interfaces describe the non-trivial conversion of a normal dissipative current into a dissipationless supercurrent. When an electron from N is injected onto a SC with an excitation energy  $|\varepsilon| < \Delta$  (the SC gap), it is reflected back as a hole with an exactly opposite direction of motion. This perfect retro-reflection process is understood as the result of the quasi-elasticity and momentum conservation of the process, combined with the fact that the hole has a negative mass. This picture is however only an approximation<sup>5</sup>. Due to a small energy loss of the electron due to its condensation into a cooper pair, the holes energy and in-plane momentum, and hence its angle of reflection, are in all generality smaller than that of the incident electron. This effect is exceedingly small in typical metallic systems where  $E_F$  strongly exceeds typical energies of  $\Delta$ , and perfect retro-AR in these systems has been confirmed in great detail<sup>6</sup>.

Recent experimental efforts however shifted towards more exotic materials such as semi-conductors<sup>7</sup>, topological insulators<sup>8</sup>, quantum Hall systems<sup>9</sup>, carbon-nanotubes<sup>10</sup> and graphene<sup>2,11</sup>. Unlike typical metals, these can have much lower  $E_F$  where the retro-reflection process can be dramatically altered. Single (SLG) and bilayer graphene (BLG)<sup>12,13</sup> with their semi-metallic band-structure and the continuous gate tunability of  $E_F$  are uniquely suited to study the  $E_F$  dependence of ARs at the cross-over from large to arbitrarily small  $E_F$ . In the recently achieved regime where  $|E_F| < \Delta^2$ , the reflected hole can undergo an inter-band transition from the conduction into the valence band, causing the holes mass to change its sign. Under these conditions, energy and momentum conservation dictate that the reflection angle becomes a non-trivial function of  $E_F$ , resulting in a spec-

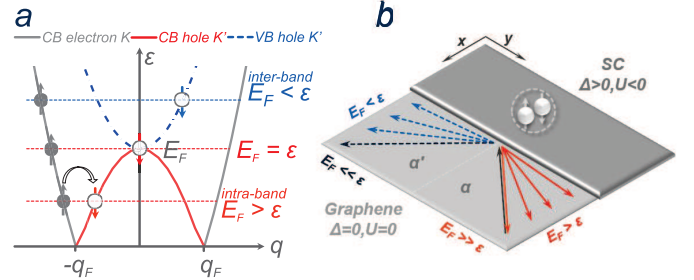


FIG. 1. (a) Excitation spectrum  $\varepsilon(q)$  for a fixed  $E_F < \Delta$ . With an increasing excitation voltage  $\varepsilon$ , the momentum in the  $y$ -direction  $q$  of the reflected hole continuously increases from negative to positive values, passing through zero when  $E_F = \varepsilon$ . (b) Schematics of the reflection angles of AR holes in the various energy limits. Starting from perfect intra-band retro-reflection in the high  $E_F$  limit, the reflection angle  $\alpha'$  continuously increases towards  $\pi/2$  as  $E_F$  is lowered. At the cross-over point separating intra-band and inter-band ARs,  $E_F = \varepsilon$ ,  $\alpha'$  exhibits a jump to  $-\pi/2$ , which eventually results in perfect inter-band specular reflection  $\alpha = \alpha'$  when  $E_F = 0$ .

ular AR process for  $E_F = 0$  where the angle of incidence and reflection are equal  $\alpha = \alpha'$  (Fig.1 (a) and (b)).

In this paper we work out a detailed analytical description of the differential conductance across a BLG/SC interface at the continuous transition from high  $|E_F| \gg \Delta$  to low  $|E_F| < \Delta$  Fermi energies. While direct measurements of scattering angles are experimentally challenging, measurements of a non-linear conductance  $G_{NS}(\varepsilon)$  as a function of the excitation energy  $\varepsilon$  are easily experimentally approachable and can illuminate the underlying scattering processes at the N/SC interface. We find two distinct regimes for  $|\varepsilon| < |E_F|$  and  $|\varepsilon| > |E_F|$  where intra-band retro-reflections and inter-band specular-reflection are taking place, respectively. We identify conductance

dips in  $G_{NS}(\varepsilon)$  at the energy condition  $|\varepsilon| = |E_F|$ , where the hole is reflected onto the charge neutrality point. This line in the energy phase space separates the two distinct regimes, so marking the cross-over from retro intra-band to specular inter-band AR.

## II. MODEL AND METHOD

We model the BLG/SC junction considering a setup similar to the one presented in the experimental device of Ref.<sup>2</sup>, and similar to the one used in the theoretical model in Ref.<sup>5</sup> (Fig. 1 (a)). We assume an impurity free BLG sheet in the half plane  $x > 0$  that has an ideal electrical contact with a SC lead at  $x < 0$ . The SC is modeled by a BLG sheet with an induced SC gap  $\Delta(x)$  that appears due to the SC proximity effect. For a more realistic BLG/SC interface we also assume that the SC contact induces an additional potential  $U(x)$  due to work-function matching of the BLG and the SC, as it is typically observed for all graphene/metal interfaces. Assuming that only singlet SC is induced and that only electrons of different valleys form Cooper pairs in the BLG, we write the Bogoliubov-deGennes (BdG) equations<sup>3</sup> that describe the electron motion in the system in the standard form

$$\begin{pmatrix} \mathcal{H}(\hat{\mathbf{K}}, x) - E_F & \Delta(x) \\ \Delta^*(x) & E_F - \mathcal{H}(\hat{\mathbf{K}}, x) \end{pmatrix} \begin{pmatrix} u \\ v \end{pmatrix} = \varepsilon \begin{pmatrix} u \\ v \end{pmatrix}, \quad (2.1)$$

where

$$\mathcal{H}(\hat{\mathbf{K}}, x) = \mathcal{H}_0(\hat{\mathbf{K}}) + U(x) \quad (2.2)$$

and  $\hat{\mathbf{K}}$  is the momentum operator.

The Hamiltonian  $\mathcal{H}_0(\mathbf{K})$  of the normal BLG for one valley is written as a  $4 \times 4$  matrix<sup>14–16</sup>

$$\mathcal{H}_0(\mathbf{K}) = \hbar v \begin{pmatrix} 0 & Ke^{i\alpha} & -t_\perp & 0 \\ Ke^{-i\alpha} & 0 & 0 & 0 \\ -t_\perp & 0 & 0 & Ke^{-i\alpha} \\ 0 & 0 & Ke^{i\alpha} & 0 \end{pmatrix} \quad (2.3)$$

where  $\alpha(\mathbf{K}) = \arctan(q/k)$  and  $K = \sqrt{k^2 + q^2}$  ( $q$  is the y-component and  $k$  is the x-component of  $\mathbf{K}$ ).

At the BLG/SC interface ( $x=0$ ) we assume a sharp potential step of  $U(x)$  and  $\Delta(x)$  :

$$U(x) = \begin{cases} -U_0, & x < 0 \\ 0, & x > 0 \end{cases}, \quad (2.4)$$

$$\Delta(x) = \begin{cases} \Delta_0 e^{i\phi}, & x < 0 \\ 0, & x > 0 \end{cases}. \quad (2.5)$$

This potential profile is clearly an oversimplification, since in the experiment these quantities can scale rather smoothly at the interface. While our assumption may result in a certain overestimation of the transmission amplitude at the interface, we do not think that the dependence of the conductance on  $E_F$  and  $\varepsilon$  can essentially be different for a smoothed potential step, and believe that this approximation should not change the basic picture of the conversion from retro- to specular ARs.

In accordance with the experimentally known parameters, we assume that the potential  $U_0$  is larger than the energies  $E_F, \Delta_0$  and  $\varepsilon$  but the largest energy in BLG is the coupling energy  $\hbar v t_\perp$  between the layers. Therefore we use the inequalities

$$\hbar v t_\perp \gg U_0 \gg E_F, \Delta_0, \varepsilon. \quad (2.6)$$

Here we want to specifically point out that the inequalities (2.6) are different from those used in Ref.<sup>17</sup>, which leads to quite different approximations and final results.

One can calculate the differential conductance  $G_{NS}(\varepsilon)$  for  $|\varepsilon| < \Delta_0$  and  $T = 0$  by considering the scattering of particles that are moving from right to left. Following the formalism of Ref.<sup>4</sup> one can solve the equations (2.1–2.6) separately for  $x > 0$  and  $x < 0$ , then match these solutions at  $x = 0$ , and so find the normal reflection  $r(\varepsilon, \alpha)$  and Andreev reflection  $r_A(\varepsilon, \alpha)$  amplitudes for all incidence angles  $\alpha$

$$\frac{G_{NS}(\varepsilon)}{G_{NN}(\varepsilon)} = \int_0^{\pi/2} (1 - r^2(\varepsilon, \alpha) + r_A^2(\varepsilon, \alpha)) \cos \alpha d\alpha, \quad (2.7)$$

where  $G_{NN}(\varepsilon)$  is the differential conductance across the interface of two normal BLG sheets.

Such a calculation is not very difficult for SLG<sup>5</sup>, however a corresponding calculation for BLG is considerably more cumbersome and it is not easy to obtain explicit formulas in all regions of the variables  $\varepsilon$  and  $E_F$ . Here we follow Beenakkers approach<sup>18</sup> that allows one to express the conductance  $G_{NS}(\varepsilon)$  in terms of transmission  $t(\varepsilon)$  and reflection  $r(\varepsilon)$  amplitudes of the scattering on the interface between two normal metals, by simply putting  $\Delta_0 = 0$ . We write the differential conductance  $G_{NS}(\varepsilon)$  in the form :

$$G_{NS}(\varepsilon) = \frac{4e^2}{h} Tr[m(\varepsilon)m^+(\varepsilon)], \quad (2.8)$$

with

$$m(\varepsilon) = t_{12}(\varepsilon)[1 - e^{-2i\beta} r_{22}^*(-\varepsilon) r_{22}(\varepsilon)]^{-1} t_{21}^*(-\varepsilon), \quad (2.9)$$

where  $\beta = \arccos(\varepsilon/\Delta_0)$ .

The conductance  $G_{NN}(\varepsilon, E_F)$  across two normal regions 1 and 2 reads

$$G_{NN}(\varepsilon, E_F) = \frac{4e^2}{h} Tr |t_{12}(\varepsilon, E_F)|^2, \quad (2.10)$$

where regions 1 and 2 correspond to N ( $x > 0$ ) and SC ( $x < 0$ ), respectively. In other words, Eq. (2.8-2.10) show that calculating the transmission  $t_{12}(\varepsilon)$ ,  $t_{21}(\varepsilon)$ , and reflection  $r_{12}(\varepsilon)$ ,  $r_{21}(\varepsilon)$  amplitudes (see Appendix) for right and left moving particles at the interface one obtains the differential conductance  $G_{NS}(\varepsilon)$  of the BLG/SC interface. The trace  $Tr$  over the scattering channels in Eqs. (2.8, 2.10) reduces to the integration over the momentum  $q$  parallel to the interface. Eqs. (2.8-2.10) also demonstrate that, in order to calculate the differential conductance  $G_{NS}$ , it is enough to understand the scattering on the interface between two normal metals, which is a considerably simpler task than calculating the differential conductance using the original formula (2.7).

Generally, one can see from Eqs. (2.8, 2.9) an important difference between the conductance of SLG and that of BLG. For SLG the energy spectrum follows the Dirac equations and hence the transmission amplitude for an electron is of order one for any  $U_0$  due to the so called Klein effect. In contrary, the spectrum of BLG is approximately quadratic and one can conclude by using standard formulas<sup>19</sup> for scattering on a step function that the transmission amplitude  $t_{12}(\varepsilon)$  decays proportionally to  $U_0^{-1/2}$  at large  $U_0$  and therefore is very small. For this reason, while the conductance  $G_{NN}$  in BLG is proportional to  $t^2$ , the conductance  $G_{NS}$  is proportional to  $t^4$ , and hence can be much smaller than  $G_{NN}$ . The presence of the SC gap can therefore strongly reduce the conductance across the interface.

In the next Section we present the main analytical formulas for the conductance leaving details of the derivation for the Appendix.

### III. ANALYTICAL EXPRESSIONS FOR THE DIFFERENTIAL CONDUCTANCE

We have to specifically distinguish between two distinct regimes :

A)  $|\varepsilon| < |E_F|$  - the reflected hole has positive energy (conduction band) and negative mass  $\Rightarrow$  intra-band retro-reflection.

B)  $|\varepsilon| > |E_F|$  - the reflected hole has negative energy (valence band) and positive mass  $\Rightarrow$  inter-band specular reflection.

#### A. $G_{NS}(\varepsilon)$ for $|\varepsilon| < |E_F|$ (retro-reflection)

Eqs. (2.8-2.10) can be rewritten using the integration over the longitudinal component  $q$  of the momentum instead of the trace over the transversal channels. How-

ever, it is even more convenient to integrate over the incident angle  $\alpha$ . The angle  $\alpha$  corresponds to the energy  $\varepsilon$ , while the reflection angle  $\alpha'$  corresponds to the energy  $-\varepsilon$ . These angles are related to each other by the condition that  $q$  is conserved during the reflection process and therefore

$$\frac{\sin \alpha'}{\sin \alpha} = -\sqrt{\frac{E_F + \varepsilon}{E_F - \varepsilon}}. \quad (3.1)$$

From this relation one can conclude that Andreev reflections are possible for the angles  $|\alpha| < \alpha_c$ , where

$$\alpha_c = \arcsin \sqrt{\frac{E_F - \varepsilon}{E_F + \varepsilon}}. \quad (3.2)$$

Writing

$$\Phi(\alpha) = \arcsin(\sin^2 \alpha), \quad (3.3)$$

$$\Phi(\alpha') = \arcsin(\sin^2 \alpha') = \arcsin \left[ \left( \frac{E_F + \varepsilon}{E_F - \varepsilon} \right) \sin^2 \alpha \right] \quad (3.4)$$

the conductance  $G_{NS}$  can be reduced to the form

$$G_{NS}(\varepsilon) = 2G_0 K_0(\varepsilon) \int_0^{\alpha_c} \frac{Y_\varepsilon(\alpha, \alpha') \cos \alpha}{2|X_\varepsilon(\alpha, \alpha')|^2} d\alpha, \quad (3.5)$$

where

$$Y_\varepsilon(\alpha, \alpha') = |t_{21}(\varepsilon)|^2 |t_{21}(-\varepsilon)|^2 \quad (3.6)$$

$$= 16L(\varepsilon) L(-\varepsilon) \cos \alpha \cos \alpha' (1 + \sin^2 \alpha) (1 + \sin^2 \alpha'),$$

$$L(\varepsilon) = \sqrt{\frac{|\varepsilon + E_F|}{U_0}} \ll 1, \quad (3.7)$$

and

$$K_0(\varepsilon) = \sqrt{|\varepsilon + E_F| t_\perp / \hbar v}. \quad (3.8)$$

The function  $X_\varepsilon(\alpha, \alpha')$  entering Eq. (3.5) equals

$$X_\varepsilon(\alpha, \alpha') = \frac{1}{2} [1 - e^{-2i\beta} r_{22}^*(-\varepsilon) r_{22}(\varepsilon)], \quad (3.9)$$

where  $\beta$  is given by the expression

$$\beta = \arccos(\varepsilon / \Delta_0). \quad (3.10)$$

Approximating this function by lowest orders in  $L(\varepsilon)$  we write

$$\begin{aligned}
|X_\varepsilon(\alpha, \alpha')|^2 &= \sin^2 \beta - 2 \sin \beta \left[ L(\varepsilon) \sqrt{1 + \sin^2 \alpha} \right. \\
&\times \sin(\beta + \Phi(\alpha)) + L(-\varepsilon) \sqrt{1 + \sin^2 \alpha'} \sin(\beta - \Phi(\alpha')) \left. \right] \\
&+ L^2(\varepsilon) (1 + \sin^2 \alpha) + L^2(-\varepsilon) (1 + \sin^2 \alpha') \\
&+ 2L(\varepsilon) L(-\varepsilon) \sqrt{(1 + \sin^2 \alpha) (1 + \sin^2 \alpha')} \\
&\times \left[ \cos(2\beta - \Phi(\alpha') + \Phi(\alpha)) - 2 \sin \Phi(\alpha) \sin \Phi(\alpha') \right]
\end{aligned} \tag{3.11}$$

The quadratic terms in  $L(\varepsilon)$ ,  $L(-\varepsilon)$  have been kept in  $|X_\varepsilon(\alpha, \alpha')|^2$  because they are the only contributions that do not vanish at  $\beta \rightarrow 0$ . In principle, there are also quadratic terms proportional to  $\sin \beta$ , but they can be neglected.

### B. $G_{NS}(\varepsilon)$ for $|\varepsilon| > |E_F|$ (specular reflection)

In this case the angles  $\alpha$  and  $\alpha'$  are related to each other as

$$\frac{\sin \alpha'}{\sin \alpha} = \sqrt{\frac{\varepsilon + E_F}{\varepsilon - E_F}} \tag{3.12}$$

and the critical angle  $\alpha_c$  equals to

$$\alpha_c = \arcsin \sqrt{\frac{\varepsilon - E_F}{\varepsilon + E_F}} \tag{3.13}$$

For  $\Phi(\alpha)$  we have the same relation as in Eq. (3.3) and obtain for  $\Phi(\alpha')$

$$\Phi(\alpha') = \arcsin \left[ \left( \frac{\varepsilon + E_F}{\varepsilon - E_F} \right) \sin^2 \alpha \right] \tag{3.14}$$

The conductance  $G_{NS}(\varepsilon)$  is then determined as before by Eq. (3.5). For the function  $Y_\varepsilon(\alpha, \alpha')$  we therefore have

$$\begin{aligned}
Y_\varepsilon(\alpha, \alpha') &= |t_{21}(\varepsilon)|^2 |t_{21}(-\varepsilon)|^2 \\
&= 16L(\varepsilon) L(-\varepsilon) \cos \alpha (1 + \sin^2 \alpha) \cos \alpha' \sin^2 \alpha'
\end{aligned} \tag{3.15}$$

The function  $X_\varepsilon(\alpha, \alpha')$  is determined from Eq. (3.9) and we obtain :

$$\begin{aligned}
|X_\varepsilon(\alpha, \alpha')|^2 &= \sin^2 \beta - 2 \sin \beta \left[ L(\varepsilon) \sqrt{1 + \sin^2 \alpha} \right. \\
&\times \sin(\beta + \Phi(\alpha)) - L(-\varepsilon) \cos \alpha' \cos(\beta + \Phi(\alpha')) \left. \right] \\
&+ 2L(\varepsilon) L(-\varepsilon) \sqrt{1 + \sin^2 \alpha} \cos \alpha' \\
&\times \left[ \sin(2\beta + \Phi(\alpha) + \Phi(\alpha')) - 2 \cos \phi(\alpha) \sin \Phi(\alpha') \right] \\
&+ L^2(\varepsilon) (1 + \sin^2 \alpha) + L^2(-\varepsilon) \cos^2 \alpha'
\end{aligned} \tag{3.16}$$

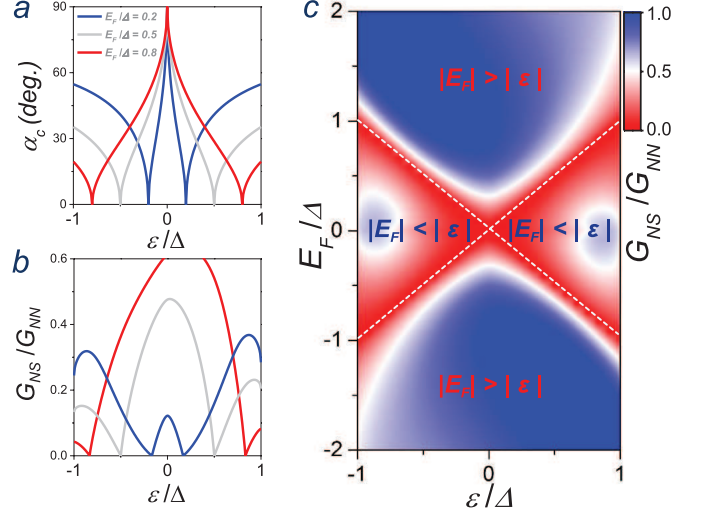


FIG. 2. (a) Angle of total internal reflection for ARs  $\alpha_c$  for various fixed  $E_F$ . For  $\varepsilon = 0$ ,  $\alpha_c = \pi/2$ , and ARs are possible for all angles of incidence. For  $\varepsilon = E_F$ , AR are prohibited for all angles and  $\alpha_c = 0$ . (b) Conductance  $G_{NS}/G_{NN}(10K)$  as a function as a function of  $\varepsilon$  for the same  $E_F$  as in (a). The conductance is pinched off at same positions at which  $\alpha_c = 0$ . (c) 2D colormap of  $G_{NS}/G_{NN}(10K)$  for a function of both  $\varepsilon$  and  $E_F$ . The conductance dips scale along the diagonal lines defined by the condition  $|\varepsilon| = |E_F|$  and define a phase diagram that separates the map into regions of retro- and specular-ARs. Here we used the parameter  $U_0 = 5\text{meV}$ .

### C. Conductance $G_{NN}$ of the interface between two normal metals

The transmission amplitude  $t_{12}(\varepsilon)$  determines the zero temperature conductance  $G_{NN}(\varepsilon)$  between two normal metals entering Eq. (2.10). At a fixed  $E_F$  the conductance  $G_{NN}(\varepsilon)$  is given by the following formula

$$G_{NN}(\varepsilon) = G_0 K_0(\varepsilon) \int_{-\pi/2}^{\pi/2} |t_{12}(\varepsilon)|^2 \cos \alpha d\alpha, \tag{3.17}$$

The final form of the conductance  $G_{NN}(\varepsilon)$  between the normal metals can be written as

$$\begin{aligned}
G_{NN}(\varepsilon) &= G_0 K_0(\varepsilon) \int_{-\pi/2}^{\pi/2} 4L(\varepsilon) \cos^2 \alpha (1 + \sin^2 \alpha) d\alpha \\
&= \frac{5\pi}{2} G_0 K_0(\varepsilon) L(\varepsilon)
\end{aligned} \tag{3.18}$$

The formulas presented in this Section describe the conductances for all parameters of interest and one can explicitly compare the corresponding numerical curves with experimental results. All the details of the derivation of the results of the present Section can be found in Appendix.

#### IV. NUMERICAL STUDY AND DISCUSSION

In the AR process the incident electron has a total energy of  $E_F + \varepsilon$  and condenses into a Cooper pair with a total energy of  $2E_F$  after transmission into the SC. Here energy conservation dictates that the reflected hole has a slightly lower total energy of  $E_F - \varepsilon$ . This energy loss of  $2\varepsilon$  can have dramatic consequences for an ultra-low  $E_F$ , where for the condition  $|\varepsilon| > E_F$ , the incident conduction hole electron can be reflected as a hole in the valence band (Fig. 1 (a) and (b)).

Due to momentum conservation parallel to the interface  $q$ , the reduced energy of the hole directly translates into an altered angle of reflection  $\alpha'$  as compared to the angle of incidence  $\alpha$ . As was shown in the previous section, these angles are related to each other by the simple relation (3.1) from which one can conclude that ARs are only possible for angles  $\alpha < \alpha_c$ , where  $\alpha_c$ , Eq. (3.2), plays the role of the angle of total internal reflection for ARs and is plotted in Fig. 2 (a) for various fixed  $E_F$ . As can be seen from the plots, for  $\varepsilon = 0$ ,  $\alpha_c = \pi/2$ , and ARs are possible for all angles of incidence. However when  $\varepsilon = E_F$ ,  $\alpha_c = 0$ , and AR are prohibited for all angles.

The explicit analytical formula for  $G_{NS}$ , Eq. (3.5), and subsequent formulas for the functions entering this equation allows us to numerically calculate  $G_{NS}(\varepsilon, E_F)$  for the full phase space. Here we explicitly calculate the normalized conductance,  $G_{NS}(\varepsilon, E_F)/G_{NN}(\varepsilon, E_F, T)$ , since this allows to better highlight the conductance features that arise solely from the SC proximity effect. As both  $G_{NS}$  and  $G_{NN}$  in a realistic sample are generally subjected to effect of energy fluctuations and disorder, one can eliminate these undesired and hard to quantify effects by simply dividing these out. Since measurements of the SC state are typically performed at  $T \ll T_c^2$ , one can use  $G_{NS}(\varepsilon, E_F)$  at  $T = 0$ , with a reasonable accuracy. However, we specifically derive a temperature broadened form of  $G_{NN}(\varepsilon, E_F, T)$  since in an experiment one can only obtain this quantity at elevated temperatures  $T > T_c$

$$G_{NN}(\varepsilon, E_F, T) = \frac{5\pi}{4} \int_{-\infty}^{\infty} \frac{K_0(\varepsilon)L(\varepsilon)dE_F}{4T \cosh^2(\frac{E_F - \varepsilon}{2T})}. \quad (4.1)$$

In Fig. 2 (b) we plot out  $G_{NS}/G_{NN}(10K)$  (here we choose  $T = 10K$  for  $G_{NN}$  as was used in Ref.<sup>2</sup>) as a function of  $\varepsilon$  for various fixed  $E_F$ . Since  $\alpha_c = 0$  for  $|\varepsilon| = |E_F|$ , it can be seen from Eq. (3.5) that the conductance vanishes,  $G_{NS} = 0$ , at these points. As discussed earlier, this condition coincides exactly with the condition that separates intra-band retro- from inter-band specular reflections. The depleted interfacial resistance for this energy condition marks therefore the cross-over between the two different regimes, and so provides a strong experimental observable. In Fig. 2 (c) we plot a 2D colormap of  $G_{NS}/G_{NN}$  for a function of both  $\varepsilon$  and  $E_F$ . The conductance dips scale along the diagonal lines defined by the condition  $|\varepsilon| = |E_F|$  and define a striking cross-like

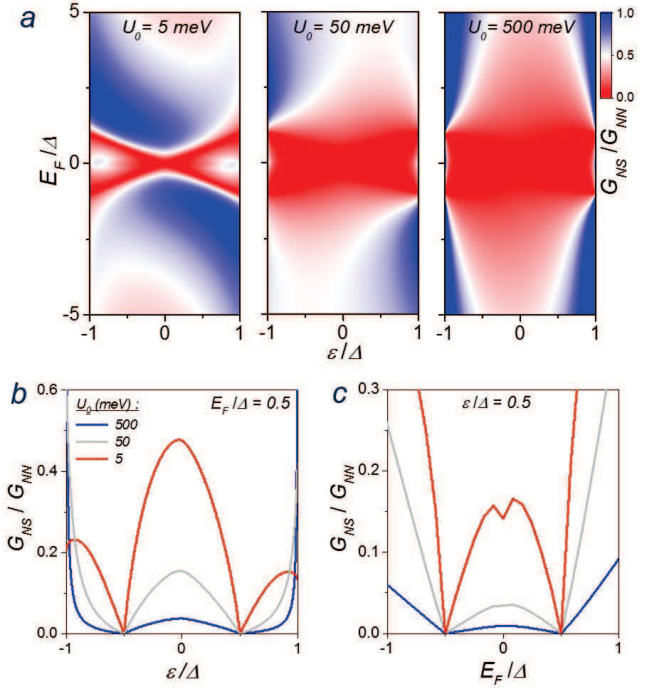


FIG. 3. Normalized conductance  $G_{NS}/G_{NN}(10K)$  for 3 different values of the potential step at the N/SC interface  $U_0$ . As can be seen from the various graphs, the inner gap conductance is strongly reduced for higher values of  $U_0$ . This results in the strong suppression of the sharpness and contrast of the characteristic cross-over point from retro- to specular ARs,  $E_F = \varepsilon$ . (a) 2D colorplots as a function of  $\varepsilon$  and  $E_F$ . (b) Excitation energy dependence  $\varepsilon$  for a fixed  $|E_F| < \Delta$ . (c) Fermi energy dependence  $E_F$  for a fixed  $|\varepsilon| < \Delta$ .

shape. One can use this map as a phase diagram to separate the region of retro- and specular-ARs.

The integrand in Eqs. (2.8, 3.5) contains only one unknown parameter, the potential step at the BLG/SC interface  $U_0$  (in Fig. 2 we used a  $U_0 = 5\text{meV}$ ). In principle, this value can be found in literature for various materials or can be extracted by fitting the experimental curves with the presented theory. In general, it is important to emphasize the role of  $U_0$  for the purpose of experiments, as it can strongly affect the outcome. In Fig. 3 we study the normalized conductance  $G_{NS}/G_{NN}$  for various values of  $U_0$ . One can see that the inner gap conductance is strongly reduced for higher values of  $U_0$ . This results in the strong suppression of the sharpness and contrast of the characteristic cross-over point from retro- to specular ARs,  $E_F = \varepsilon$ . This suppression can be explained by the previously discussed decaying transmission amplitude  $t_{12}(\varepsilon)$  which scales proportionally to  $U_0^{-1/2}$  and is therefore very small for large  $U_0$ . For experimental studies of specular AR in BLG/SC junctions it is therefore important to engineer an interface with a rather small potential step  $U_0$ .

## V. CONCLUSIONS

In this manuscript we have rigorously worked out analytical expressions for the differential conductance across a BLG/SC interface for the ultimate limits of large and small Fermi energies  $E_F$ . We have found, that while for  $E_F \gg \Delta$  the AR process is described by intra-band retro-reflections, in the limit of  $E_F \ll \Delta$  they are described by inter-band specular-reflections. From numerical calculations we find that the cross-over between the two processes has a clear experimental signature that manifests itself in a strongly suppressed interfacial conductance when the excitation energy  $|\varepsilon| = |E_F| < \Delta$ .

## VI. ACKNOWLEDGEMENTS

The authors thank C. W. J. Beenakker, P. Kim and J. D. Pillet for helpful discussions. K.B. Efetov gratefully acknowledges the financial support of the Ministry of Education and Science of the Russian Federation in the framework of Increase Competitiveness Program of NUST “MISIS” (Nr. K2-2014-015) and Priority Program 1459 “Graphene” of *Deutsche Forschungsgemeinschaft*.

## VII. APPENDIX : EIGENENERGIES, WAVE FUNCTIONS, TRANSMISSION AND REFLECTION AMPLITUDES IN THE ABSENCE OF A SC GAP

Equations (2.8-2.10) allow one to reduce the calculation of the conductance of the N/SC junction to study of the transmission and reflection amplitudes between two normal metals. This can be done putting  $\Delta = 0$  in Eqs. (2.1-2.3) and writing the obtained equation in the form :

$$\left( \mathcal{H}_0(\hat{\mathbf{K}}) + U(x) \right) u = E u, \quad (7.1)$$

with  $U(x)$  defined in Eq. (2.4). One should now solve Eqs. (7.1) separately at  $x > 0$  and  $x < 0$  and match the solutions at  $x = 0$ .

### A. Eigenenergies

First, following Refs.<sup>14-16</sup>, we write the eigenenergies  $E(\mathbf{K})$  of the Hamiltonian  $\mathcal{H}_0(\mathbf{K})$ , Eq. (2.3), for an arbitrary relation between  $t_\perp$  and the characteristic energies inside one layer in the form :

$$\begin{aligned} E_1(\mathbf{K}) &= \hbar v (-t_\perp/2 - \mathcal{E}(\mathbf{K})), \\ E_2(\mathbf{K}) &= \hbar v (-t_\perp/2 + \mathcal{E}(\mathbf{K})), \\ E_3(\mathbf{K}) &= \hbar v (t_\perp/2 + \mathcal{E}(\mathbf{K})), \\ E_4(\mathbf{K}) &= \hbar v (t_\perp/2 - \mathcal{E}(\mathbf{K})), \end{aligned} \quad (7.2)$$

where

$$\mathcal{E}(\mathbf{K}) = \sqrt{(t_\perp/2)^2 + K^2} \quad (7.3)$$

Provided the interlayer coupling  $t_\perp$  exceeds all the other energies, the bands of the Hamiltonian (2.3) with the spectra  $E_1(\mathbf{k})$  and  $E_3(\mathbf{k})$  are far away from the Fermi energy and their contribution into physical quantities can be neglected. The eigenenergies of the first two low energy bands take in the limit of small  $|\mathbf{k}| \ll t_\perp$  the following form:

$$\begin{aligned} E_2(\mathbf{k}) &= \hbar v (-t_\perp/2 + \mathcal{E}(\mathbf{k})) \approx \frac{\hbar v K^2}{t_\perp}, \\ E_4(\mathbf{k}) &= \hbar v (t_\perp/2 - \mathcal{E}(\mathbf{k})) \approx -\frac{\hbar v K^2}{t_\perp}. \end{aligned} \quad (7.4)$$

In Eq. (7.4),  $E_2(\mathbf{K})$  describes the conduction band and  $E_4(\mathbf{K})$  describes the valence band. Using the inequality (2.6) we consider only these low-lying bands and no higher energy bands.

### B. Wave functions

The Hamiltonian  $\mathcal{H}_0(\mathbf{k})$ , Eq. (2.3), can be diagonalized as was done in Ref.<sup>16</sup>, and we can easily obtain 4-component vectors  $u$  that satisfy the equation

$$(\mathcal{H}(\mathbf{k}) - E_F) u = \varepsilon u. \quad (7.5)$$

Here we consider only the case  $E_F > 0$ . The solutions depend on the sign of  $\varepsilon + E_F$  and we write them separately for  $\varepsilon + E_F > 0$  and  $\varepsilon + E_F < 0$ .

For the low-lying eigenvalues we obtain

$$\varepsilon_2 = -E_F + \frac{\hbar v}{t_\perp} K^2, \quad (7.6)$$

$$\varepsilon_4 = -E_F - \frac{\hbar v}{t_\perp} K^2 \quad (7.7)$$

In order to calculate the wave functions one should choose an eigenvalue  $\varepsilon$  and determine  $K$  as a function of this  $\varepsilon$ . It is clear that constructing plain waves in the region of the normal metal  $N_1$  and  $E_F > 0$  one should take the solution of Eq. (7.6) for  $K$  as a function of  $\varepsilon$  at  $\varepsilon > -E_F$  and of Eq. (7.7) at  $\varepsilon < -E_F$ . In addition, one has a solution for  $K$  of (7.7) at  $\varepsilon > -E_F$  and of (7.6) at  $\varepsilon < -E_F$ . The latter solutions are either exponentially growing or decaying as functions of  $x$ . Nevertheless, they should also be taken into account when matching functions at the interface because we have the deep potential  $-U_0$  at  $x < 0$  and the exponential growth can change to the plain wave behavior there.

Here we calculate the wave functions for the region  $x > 0$ . These can be however also used in the region

$x < 0$  after shifting the energy  $E_F \rightarrow E_F + U_0$ . We will later on denote all quantities where this shift has been done by adding the subscript  $U_0$ , thus obtaining  $u_{1U_0}^{R,L}$ ,  $u_{2U_0}^{R,L}$ , etc.

### 1. Plain wave solutions at $\varepsilon + E_F > 0$

In this region of the energies we have left and right moving electrons of the conduction band and use Eq. (7.6). The solution  $u_1^R$  for right moving particles in this region takes the form :

$$u_1^R = \frac{e^{ikx+iqy}}{2\sqrt{K_0/t_\perp \cos \alpha}} \begin{pmatrix} K_0/t_\perp \\ e^{-i\alpha} \\ K_0/t_\perp \\ e^{i\alpha} \end{pmatrix}, \quad (7.8)$$

while the solution for the left moving particles  $u_1^L$  reads (we use a compact notation  $K_0 = K_0(\varepsilon)$ , Eq. (3.8))

$$u_1^L = \frac{e^{-ikx+iqy}}{2\sqrt{K_0/t_\perp \cos \alpha}} \begin{pmatrix} -K_0/t_\perp \\ e^{i\alpha} \\ -K_0/t_\perp \\ e^{-i\alpha} \end{pmatrix}. \quad (7.9)$$

The wave functions  $u_1^R$  and  $u_1^L$  correspond to the eigenenergy  $E_2(\mathbf{k})$ , Eq. (7.4), and belong to the conduction band. They are normalized assuming the current 1 along the  $x$ -axis for the right moving particles and  $-1$  for left moving ones. This fact can easily be checked using the matrix form of the current operator

$$\mathbf{j} = e\sigma \quad (7.10)$$

having the  $x$ -component

$$j_x = e\sigma_x, \quad (7.11)$$

where  $\sigma$  is the vector of Pauli matrices in the sublattice space of graphene.

Having fixed  $E_F > 0$  we have to express  $k$  and  $q$  in terms of  $K_0$  and  $\alpha$ . Since we introduced the angle  $\alpha$  as

$$k - iq = K_0 e^{-i\alpha}, \quad (7.12)$$

we obtain for  $\varepsilon + E_F > 0$  the following relations for the variables  $\alpha$  and  $k$

$$k = K_0 \cos \alpha, \quad q = K_0 \sin \alpha \quad (7.13)$$

Here the angle  $\alpha$  varies in the interval  $-\pi/2 < \alpha < \pi/2$ .

### 2. Plain wave solutions at $\varepsilon + E_F < 0$

In this region of energies we have plain waves corresponding to right and left moving holes from the valence band and use Eq. (7.7). For the right moving holes we obtain the normalized wave functions :

$$u_2^R = \frac{e^{ik'x+iqy}}{2\sqrt{K_0/t_\perp \cos \alpha'}} \begin{pmatrix} K_0/t_\perp \\ e^{-i\alpha'} \\ -K_0/t_\perp \\ -e^{i\alpha'} \end{pmatrix}, \quad (7.14)$$

where

$$k' = -K_0 \cos \alpha', \quad q = -K_0 \sin \alpha'. \quad (7.15)$$

In Eqs. (7.14, 7.15), the angle  $\alpha'$  varies in the interval  $-\pi/2 < \alpha' < \pi/2$ .

The opposite signs in Eq. (7.15), as compared to Eq. (7.13), are due to the fact that we now consider holes from the valence band instead of electrons from the conduction band.

The solution  $u_2^L$  for the left moving particles takes the form

$$u_2^L = \frac{e^{-ik'x+iqy}}{2\sqrt{K_0/t_\perp \cos \alpha'}} \begin{pmatrix} -K_0/t_\perp \\ e^{i\alpha'} \\ K_0/t_\perp \\ -e^{-i\alpha'} \end{pmatrix}. \quad (7.16)$$

The current of the right moving holes (functions  $u_2^R$ ) equals 1, while the current for the left moving holes (function  $u_2^L$ ) equals  $-1$ .

### 3. Decaying and growing solutions at $\varepsilon + E_F < 0$

In addition to the plain waves, Eqs. (7.8, 7.9), there are two other solutions  $u_1^<$  and  $u_1^>$  corresponding to the eigenvalue  $\varepsilon_2$ , Eq. (7.6) from the conduction band :

$$u_1^< = e^{\kappa x+iqy} \begin{pmatrix} -iK_0/t_\perp \\ e^\gamma \\ -iK_0/t_\perp \\ e^{-\gamma} \end{pmatrix} \quad (7.17)$$

and

$$u_1^> = e^{-\kappa x+iqy} \begin{pmatrix} iK_0/t_\perp \\ e^{-\gamma} \\ iK_0/t_\perp \\ e^\gamma \end{pmatrix} \quad (7.18)$$

The normalization in Eq. (7.17, 7.18) does not play any role and we just set it equal to unity. The parameters  $\kappa$  and  $q$  can be written in the form :

$$\kappa = K_0 \cosh \gamma, \quad q = K_0 \sinh \gamma \quad (7.19)$$



#### 4. Decaying and growing solutions at $\varepsilon + E_F > 0$

In this region of parameters there are growing and decaying wave functions that correspond to  $\varepsilon_4$  from Eq. (7.7) and belong to the valence band. We write the growing  $u_2^<$  and decaying  $u_2^>$  functions as

$$u_2^< = e^{\kappa x + i q y} \begin{pmatrix} i K_0 / t_\perp \\ e^{\gamma'} \\ -i K_0 / t_\perp \\ -e^{-\gamma'} \end{pmatrix} \quad (7.20)$$

and

$$u_2^> = e^{-\kappa x + i q y} \begin{pmatrix} -i K_0 / t_\perp \\ e^{-\gamma'} \\ i K_0 / t_\perp \\ -e^{\gamma'} \end{pmatrix} \quad (7.21)$$

The parameters  $\kappa$  and  $q$  can be written in the form

$$\kappa = K_0 \cosh \gamma', \quad q = K_0 \sinh \gamma' \quad (7.22)$$

#### 5. Relations between the variables $\alpha, \alpha'$ and $\gamma', \gamma$

The variables  $\alpha, \alpha', \gamma$  and  $\gamma'$  are not independent because the component  $q$  parallel to the interface is everywhere the same. Comparing Eqs. (7.13) and (7.22) we come to the relation :

$$\sin \alpha = \sinh \gamma', \quad (7.23)$$

while the comparison of Eqs. (7.15) and (7.19) leads to

$$\sin \alpha' = -\sinh \gamma \quad (7.24)$$

#### C. Transmission $t_{21}(\varepsilon), t_{12}(\varepsilon)$ and reflection $r_{21}(\varepsilon)$ amplitudes

Now we calculate the transmission  $t_{21}(\varepsilon)$  and reflection  $r_{21}(\varepsilon)$  amplitudes that match the wave functions written on the left and on the right from the interface. Again, we consider the regions  $\varepsilon + E_F > 0$  and  $\varepsilon + E_F < 0$  separately. Then, the transmission amplitude  $t_{12}(\varepsilon)$  can easily be obtained from  $t_{21}(\varepsilon)$  through the well know relation

$$t_{12}(\varepsilon) = t_{21}(\varepsilon) e^{i\delta(\varepsilon)}, \quad (7.25)$$

where  $\delta(\varepsilon)$  is a phase whose explicit value is not necessary for the calculation of the conductances using Eqs. (2.8-2.10).

#### 1. Region $E_F > 0, \varepsilon + E_F > 0$

The scattering process at  $x < 0$  includes a plane wave that is incident from the left,  $u_{1U_0}^R$ , and another one,  $u_{1U_0}^L$ , reflected from the interface. In addition, in the region  $x < 0$  one has a wave that is growing with  $x$  (decaying from the interface) with the symmetry of  $u_1^<$  from Eq. (7.17).

After scattering off the interface one obtains an outgoing wave for  $x > 0$  with the structure  $u_1^R$ , Eq. (7.8), and a decaying wave with the structure  $u_2^>$ , Eq. (7.21). We describe the scattering process for  $\varepsilon + E_F > 0$  that matches these functions at the interface :

$$u_{1U_0}^R + r_{22}(\varepsilon) u_{1U_0}^L + B u_{2U_0}^< = t_{21}(\varepsilon) u_1^R + C u_2^>, \quad (7.26)$$

where  $B$  and  $C$  are coefficients have to be found by solving Eq. (7.26). Actually, Eq. (7.26) is a system of 4 linear equations and one has to find four unknown quantities  $r_{22}(\varepsilon)$ ,  $t_{21}(\varepsilon)$ ,  $B(\varepsilon)$  and  $C(\varepsilon)$ .

Writing Eqs. (7.26) explicitly leads to some quite cumbersome expressions. Fortunately, these equations are simpler in the limit  $U_0 \gg \varepsilon, E_F$ , which is explicitly considered here. The amplitudes  $t_{21}(\varepsilon)$  and  $r_{22}(\varepsilon)$  can now be found rather easily. Using Eq. (3.7) we write

$$\frac{\sin \alpha(U_0)}{\sin \alpha} \simeq \sqrt{\frac{\varepsilon + E_F}{U_0}} = L(\varepsilon) \ll 1 \quad (7.27)$$

to obtain in the linear approximation in  $\alpha$

$$\cos \alpha(U_0) = \sqrt{1 - L^2(\varepsilon) \sin^2 \alpha} \simeq 1. \quad (7.28)$$

We can hence approximate

$$e^{i\alpha(U_0)} \simeq 1 + iL(\varepsilon) \sin \alpha, \quad e^{\gamma(U_0)} = 1 + L(\varepsilon) \sinh \gamma. \quad (7.29)$$

and simplify Eqs. (7.26) with the help of the relations (7.27-7.29). We solve these equations and arrive at the following expression for the transmission coefficients  $t_{21}(\varepsilon)$  and  $r_{22}(\varepsilon)$  :

$$t_{21}(\varepsilon) = \frac{2\sqrt{L(\varepsilon)} \cos \alpha \cosh \gamma'}{\cos \alpha \cosh \gamma' + i \sin \alpha \sinh \gamma'}, \quad (7.30)$$

and

$$r_{22}(\varepsilon) = 1 - \frac{2L(\varepsilon) \cosh \gamma'}{\cos \alpha \cosh \gamma' + i \sin \alpha \sinh \gamma'} \quad (7.31)$$

Using Eq. (7.27) we rewrite Eqs. (7.30-7.31) in a more compact form

$$t_{21}(\varepsilon) = 2\sqrt{L(\varepsilon) \cos \alpha (1 + \sin^2 \alpha)} \exp(-i\Phi(\alpha)), \quad (7.32)$$



with  $\Phi(\alpha)$  introduced in Eq. (3.3).

Since the angle  $\Phi(\alpha)$  varies in the interval

$$0 < \Phi(\alpha) < \pi/2 \quad (7.33)$$

we obtain for the reflection coefficient

$$r_{22}(\varepsilon) = 1 - 2L(\varepsilon) \sqrt{(1 + \sin^2 \alpha)} \exp(-i\Phi(\alpha)) \quad (7.34)$$

The unitarity condition immediately follows from Eqs. (7.32, 7.34) in the limit (7.27)

$$|t_{21}(\varepsilon)|^2 + |r_{22}(\varepsilon)|^2 = 1 \quad (7.35)$$

## 2. Region $E_F > 0$ , $\varepsilon + E_F < 0$

In the region  $E_F > 0$ ,  $\varepsilon + E_F < 0$  matching the wave functions at  $x = 0$  results in the equation :

$$u_{1U_0}^R + r_{22}(\varepsilon) u_{1U_0}^L + B(\varepsilon) u_{2U_0}^< = t_{21}(\varepsilon) u_2^R + C(\varepsilon) u_1^>, \quad (7.36)$$

Using the same approximation (7.27-7.29) and proceeding in the same way as for  $\varepsilon + E_F$  one comes with the help of Eq. (7.24) to the following result for the transmission amplitude

$$t_{21}(\varepsilon) = -2\sqrt{L(\varepsilon) \cos \alpha'} \sin \alpha' \exp(i\Phi(\alpha')) \quad (7.37)$$

The reflection amplitude  $r_{22}(\varepsilon)$  can be then written as

$$r_{22}(\varepsilon) = 1 - 2iL(\varepsilon) \cos \alpha' \exp(i\Phi(\alpha')), \quad (7.38)$$

with

$$\Phi(\alpha') = -\arcsin(\sin^2 \alpha') \quad (7.39)$$

Again, the unitarity condition, Eq. (7.35), is fulfilled in the limit specified in Eq. (7.27).

- 
- <sup>1</sup> A.F. Andreev, Zh. Eksp. Teor. Fiz. **46**, 1823 (1964) [Sov. Phys. JETP **19**, 1228 (1964)].
- <sup>2</sup> D. K. Efetov, L. Wang, C. Handschin, K. B. Efetov, J. Shuang, R. Cava, T. Taniguchi, K. Watanabe, J. Hone, C. R. Dean and P. Kim, Nature Physics, **12**, 328 (2016).
- <sup>3</sup> P.G. De Gennes, *Superconductivity of Metals and Alloys*, (Benjamin, New York, 1966).
- <sup>4</sup> G.E. Blonder, M. Tinkham, and T.M. Klapwijk, Phys. Rev. B **25**, 4515 (1982).
- <sup>5</sup> C.W.J. Beenakker, PRL **97**, 067007 (2006).
- <sup>6</sup> P. A. M. Benistant, A. P. van Gelder, H. van Kempen and P. Wyder, Physical Review B **32**, 3351(R) (1985).
- <sup>7</sup> V. Mourik, K. Zuo, S. M. Frolov, S. R. Plissard, E. P. A. M. Bakkers, L. P. Kouwenhoven, Science **336**, 1003-1007 (2012).
- <sup>8</sup> J. R. Williams, A. J. Bestwick, P. Gallagher, S. S. Hong, Y. Cui, A. S. Bleich, J. G. Analytis, I. R. Fisher, D. Goldhaber-Gordon, PRL **109**, 056803 (2012).
- <sup>9</sup> F. Amet, C. T. Ke, I. V. Borzenets, Y.-M. Wang, K. Watanabe, T. Taniguchi, R. S. Deacon, M. Yamamoto, Y. Bomze, S. Tarucha and G. Finkelstein, arXiv:1512.09083 (2015).
- <sup>10</sup> J.-D. Pillet, C. H. L. Quay, P. Morfin, C. Bena, A. Levy Yeyati and P. Joyez, Nature Physics **6**, 965969 (2010).
- <sup>11</sup> H.B. Heersche, P. Jarillo-Herrero, J.B. Oostinga, L.M.K. Vandersypen, and A. F. Morpurgo, Nature **446**, 56 (2007).
- <sup>12</sup> K.S. Novoselov, A.K. Geim, S.V. Morozov, D. Jiang, M.I. Katsnelson, I.V. Grigorieva, S.V. Dubonos, and A.A. Firsov, Nature **438**, 197 (2005).
- <sup>13</sup> Y. Zhang, Y.-W. Tan, H. L. Stormer, and P. Kim, Nature **438**, 201 (2005).
- <sup>14</sup> P.R. Wallace, Phys. Rev. **71**, 622 (1947).
- <sup>15</sup> E. McCann and V.I. Fal'ko, Phys. Rev. Lett. **96**, 086805 (2006).
- <sup>16</sup> J. Nilsson, A.H. Castro Neto, N.M.R. Peres, and F. Guinea, Phys. Rev. B **73**, 214418 (2006).
- <sup>17</sup> T. Ludwig, Phys. Rev. B **75**, 195322 (2007).
- <sup>18</sup> C.J.W. Beenakker, Rev. Mod. Phys. **69**, 731 (1997).
- <sup>19</sup> L.D. Landau, E.M. Lifshitz. *Course of Theoretical Physics, Vol 3*, Pergamon Press (1977).
- <sup>20</sup> We want to mention that the conductance across a BLG/SC interface was already calculated in Ref. 17. However, the calculations in that publication were done assuming that the potential  $U_0$  is highest energy in the system and explicit results were written only in some limiting case. In contrast, we use a more relevant assumption that the potential  $U_0$  is smaller than the interlayer coupling energy and derive general formulas that allow us to make the comparison with the experiment<sup>2</sup> in the entire region of the parameters  $\varepsilon$  and  $E_F$ .